

1 Ocean warming threatens the viability of 60% of  
2 Antarctic ice shelves

3 C. Burgard<sup>1,2\*</sup>, N.C. Jourdain<sup>2</sup>, C. Mosbeux<sup>2</sup>, J. Caillet<sup>2</sup>,  
4 P. Mathiot<sup>2</sup>, C. Kittel<sup>2,3,4</sup>

5 <sup>1\*</sup>Laboratoire d'Océanographie et du Climat: Expérimentations et  
6 Approches Numériques (LOCEAN), Sorbonne  
7 Université/CNRS/IRD/MNHN, Paris, France.

8 <sup>2</sup>IGE, Univ. Grenoble Alpes/IRD/CNRS/INRAE/Grenoble INP,  
9 Grenoble, France.

10 <sup>3</sup>ULiège, Department of Geography, UR SPHERES, Liège, Belgium.

11 <sup>4</sup>Vrije Universiteit Brussel, Physical Geography Research Group,  
12 Department of Geography, Brussels, Belgium.

13 \*Corresponding author(s). E-mail(s): [clara.burgard@locean.ipsl.fr](mailto:clara.burgard@locean.ipsl.fr);

14 **Abstract**

15 The disappearance of ice shelves, the floating margins of the Antarctic ice sheet  
16 that restrain the ice flow into the ocean, would strongly accelerate the Antarctic  
17 contribution to sea-level rise. Their viability in a warming world has motivated  
18 a lot of work, with a strong focus on the influence of the warming atmosphere.  
19 We revisit the concept of ice-shelf viability in a holistic manner, taking into  
20 account mass loss due to both the atmosphere and the ocean, to estimate when  
21 it becomes virtually impossible for the ice shelves to maintain their present-day  
22 shape. For a scenario remaining largely below 2°C of global warming, only one  
23 out of 64 ice shelves likely becomes non-viable by 2300. For a scenario reaching  
24 nearly 12°C of global warming by 2300, many ice shelves become non-viable once  
25 global warming exceeds 4.5°C, mainly due to an increase in ocean-induced melt.  
26 26 ice shelves are likely non-viable by 2150, and 38 in 2300. Ice-sheet regions  
27 restrained by these 38 ice shelves represent a sea-level rise potential of 10 m. Our  
28 estimates are latest bounds for reaching non-viability and ice-shelf collapse could  
29 occur even earlier, in particular due to the synergy with hydrofracturing.

30 **Keywords:** Antarctica, Climate change, Ice shelves, Modeling

31 The Antarctic ice sheet has been losing mass at an accelerating pace, becoming a  
32 significant contributor to global sea-level rise [1]. Ice shelves, the floating margins of  
33 the Antarctic ice sheet, are a crucial element controlling this mass loss. As they restrain  
34 the ice flow from the grounded ice sheet to the ocean through so-called *buttressing*  
35 [2, 3], they represent a safety band around Antarctica [4]. Their thinning and eventual  
36 collapse hence accelerates the ice discharge into the ocean [5, 6] and could, in addition,  
37 trigger two instability mechanisms that accelerate Antarctic mass loss: the Marine  
38 Ice Sheet Instability (MISI) [7, 8] and the Marine Ice Cliff Instability (MICI) [9, 10].  
39 Projections assuming both instabilities to take place in the 21<sup>st</sup> century result in a  
40 global sea-level rise of up to 1.75 m until 2100 [1], threatening coastal regions all over  
41 the world.

42 Ice shelves subsist due to a fragile balance between mass gain and mass loss at  
43 their boundaries with the grounded ice sheet, the atmosphere, and the ocean. Over  
44 the past decades, when considering all of Antarctica, mass loss to the ocean through  
45 iceberg calving and ice-shelf basal melting has substantially compensated the large  
46 mass gain through the ice flow from the grounded ice sheet to the ice shelf and the  
47 minor mass gain through the atmosphere [11]. Lately, especially in the Amundsen Sea,  
48 many ice shelves have been out of balance, significantly losing mass [11, 12].

49 As anthropogenic climate change further unfolds, more and more pressure will be  
50 exerted on the ice shelves, both at their surface due to a warmer atmosphere [13, 14],  
51 and at their base due to more intrusions of warm water [15, 16], leading to ice-shelf  
52 thinning and retreat. At the same time, the thinning of an ice shelf usually reduces  
53 buttressing, leading to a faster ice flow from the grounded ice sheet to the ice shelf [8],  
54 which tends to make the ice shelf thicker. The competing evolution of such processes  
55 will drive the evolution of ice shelves and their potential disappearance in the next  
56 decades to centuries. Here, we examine if, when, and why ice shelves will no longer  
57 be viable, at the latest, due to changes in atmosphere and ocean conditions.

## 58 Estimating non-viability

59 Since the 1960s, the idea of a climatic limit of viability for ice shelves has been  
60 explored, based on the observation that temperate ice shelves (close to their freezing  
61 temperature) do not exist and that the warmest parts of the Antarctic Peninsula  
62 are free of ice shelves [17, 18]. A limit based on an air-temperature threshold was  
63 suggested and further refined when several ice shelves of the Antarctic Peninsula  
64 retreated in the late 1990s and early 2000s [19, 20]. The collapse of Larsen A-B in  
65 1995 and Larsen B in 2002 highlighted the importance of hydrofracturing [21–23]  
66 for the viability of ice shelves. Hydrofracturing occurs when surface meltwater favors  
67 the propagation of crevasses and eventual disintegration of the ice shelf. However,  
68 hydrofracturing can only take place if the ice shelf is sufficiently weak [24]. Ice-shelf  
69 thinning due to changes in ocean or atmosphere conditions can provide the necessary  
70 mechanical preconditioning [25–27].

71 The progressive fragmentation of Thwaites glacier’s western tongue from approx-  
72 imately 2009 [28] showed that an ice-shelf collapse can even occur in the absence of  
73 surface meltwater [29, 30]. It was driven by a combination of ocean-induced ice-shelf  
74 thinning [31, 32] and increased ice damage [33]. These elements prove that the limit  
75 of viability for ice shelves cannot be defined solely from air temperature or surface  
76 melt rates.

77 We therefore revisit the concept of ice-shelf viability in a holistic approach, includ-  
78 ing all terms contributing to the Antarctic ice-shelf mass balance (Fig. 1): the flux  
79 from the grounded ice sheet to the floating ice shelf (called grounding-line flux here-  
80 after), the iceberg calving flux at the ice-shelf front, the surface mass balance (the  
81 difference between surface accumulation and ablation), and the basal mass balance  
82 (the difference between basal melting and refreezing). We define the limit of viability  
83 as the moment where mass loss at the surface, at the base, and at the front exceeds  
84 the maximum possible incoming grounding-line flux. This is done for the individual

85 ice shelves and under different greenhouse gas emission scenarios. The maximum pos-  
86 sible grounding-line flux corresponds to the flux in the absence of ice-shelf buttressing,  
87 i.e. the flux that would occur immediately after an abrupt ice-shelf collapse with max-  
88 imal damage. We use it so that we do not have to rely on the transient evolution of  
89 ice-sheet models in which ice-shelf calving and damage are either poorly or not repre-  
90 sented [34]. Our limit of viability thus represents the ocean and atmosphere conditions  
91 for which it is virtually impossible that an ice shelf maintains its current shape on the  
92 long term and does not represent the actual date at which an ice shelf disintegrates  
93 or reaches zero thickness. As evolving calving and damage cannot explicitly be repre-  
94 sented, our approach provides the latest-bound conditions in which an ice shelf will  
95 be significantly weakened due to long-term thinning and therefore more vulnerable to  
96 disintegration.

97 We derive mass loss and gain at the interface with ocean and atmosphere based on  
98 a range of climate simulations [35] covering 1850 to 2300 under two future-emission  
99 scenarios. In the low-emission scenario, global warming remains below 2°C until 2300.  
100 In the high-emission scenario, global warming reaches nearly 12°C by 2300. On the  
101 atmospheric side, we use regional climate model simulations [13, 36] of the surface  
102 mass balance driven by the global climate simulations. On the oceanic side, we derive  
103 the basal mass balance from the climate simulations using a range of parameterisa-  
104 tions based on either simple physics [37] or artificial neural networks [38]. On the ice  
105 dynamics side, we estimate the maximal grounding-line flux by simulating the instan-  
106 taneous response of the current ice sheet to a total loss of ice-shelf buttressing: using  
107 an ice-sheet model in a state constrained by observations, we remove all ice shelves  
108 at once. We repeat the experiment with three different bed plasticities to take into  
109 account uncertainty arising from ice-sheet model assumptions. As large uncertain-  
110 ties around future calving evolution remain [39, 40], we assume the lowest bound by  
111 setting calving to zero. Finally, to constrain our analysis to a plausible ensemble for

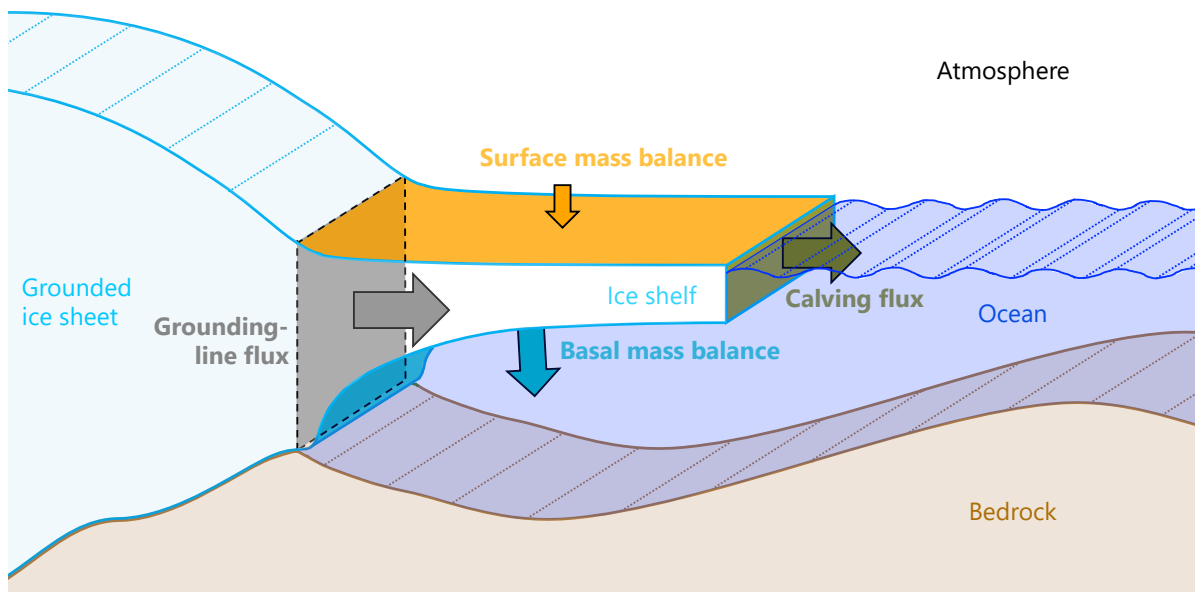


**Fig. 1 Schematic of the terms contributing to the Antarctic ice-shelf mass balance.** Due to ice dynamics, mass is gained through the grounding-line flux (the ice flow from the grounded ice sheet to the floating ice shelf) and lost through the calving of icebergs at the ice-shelf front. The surface mass balance, which describes mass exchange with the atmosphere, is determined by the difference between accumulation (mainly snowfall, but also rainfall and frost deposition) and ablation (runoff and sublimation). The basal mass balance, which describes mass exchange with the ocean, is determined by the difference between basal melting and refreezing.

112 every ice shelf, we weigh the multiple combinations of climate models, basal melt  
 113 parameterisations, and bed plasticities based on (1) their comparison to the observed  
 114 ice-shelf mass balance [11] and (2) the plausibility of the models' equilibrium climate  
 115 sensitivity [36]. More details are provided in the Methods section.

116 Our approach relies on the current ice-sheet geometry. However, repeating the anal-  
 117 ysis for two different plausible future ice-sheet geometries shows that our conclusions  
 118 remain on the conservative side, even though grounding-line retreat and increased  
 119 precipitation over the grounded ice sheet locally lead to an increase in the grounding-  
 120 line flux and its upper estimate (more details in the Methods section and in Section  
 121 5 of the Supp. Info.).

## 122 Reaching non-viability

123 The time of reaching non-viability strongly depends on the scenario (Fig. 2). While  
124 only one of the 64 ice shelves becomes likely non-viable by 2300 in the low-emission  
125 scenario, 26 become likely non-viable before 2150 in the high-emission scenario, a  
126 number that raises to 38 out of 64 by 2300. There is very high confidence on the  
127 widespread non-viability in the high-emission scenario, with 30 very likely non-viable  
128 ice shelves by 2300.

129 Looking at the projections for the low-emission scenario, the likelihood of non-  
130 viability remains nearly unchanged from present-day to the mid 23<sup>rd</sup> century. The  
131 number of ice shelves crossing the 10% and 33% likelihood of becoming non-viable  
132 increases more rapidly after 2250 (Fig. 2a), and one ice shelf becomes likely non-viable  
133 shortly before 2300. This hints at possible long-term changes in viability beyond 2300,  
134 despite a clear emission reduction and global air temperature stabilisation after 2100.

135 In the high-emission scenario, a majority of ice shelves gradually moves towards  
136 non-viability between 2050 and 2300. The period between approximately 2085 and  
137 2170 marks the period with the highest rate of ice shelves reaching likely non-viability,  
138 with 44% of the ice shelves becoming likely non-viable and 30% even very likely,  
139 over 85 years. Looking at the global surface air temperature evolution as a proxy for  
140 climate change (Fig. S1), this corresponds to crossing a threshold of  $\sim 4.5^{\circ}\text{C}$  of global  
141 warming compared to the early historical period (1850-1900).

142 This effect is widespread and not confined to a given region. Ice shelves become  
143 likely and very likely non-viable between 2100 and 2300 all around Antarctica  
144 (Fig. 2c). The main hot spots are West Antarctica, where a majority of ice shelves  
145 from the Bellingshausen Sea to the Ross Sea are likely or very likely non-viable by  
146 2200, as well as the ice shelves from the Eastern Weddell Sea to the eastern edge of  
147 Dronning Maud Land. A few other ice shelves in East Antarctica, such as West and  
148 Shackleton ice shelves, also display a very high likelihood of becoming non-viable.

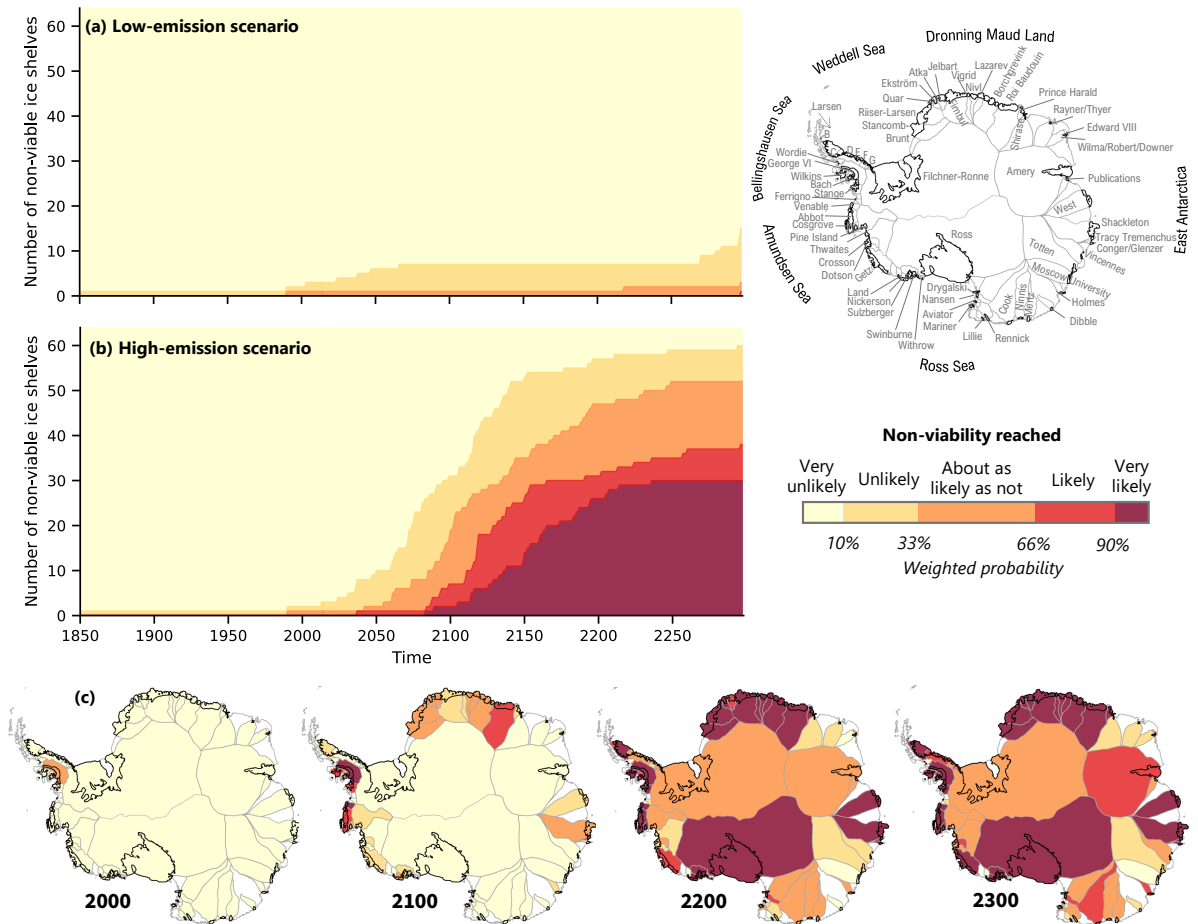


**Fig. 2** Distribution of ice-shelf non-viability over time and space. Evolution of the number of non-viable ice shelves over time for (a) the low-emission scenario and (b) the high-emission scenario over time. (c) Spatial distribution of the weighted likelihood of reaching non-viability for the years 2000, 2100, 2200 and 2300 in the high-emission scenario. The color corresponding to the likelihood is applied to the ice shelves and their associated drainage basins for more visibility. Geographical indications of the main Antarctic regions, ice shelves (black contours) and associated drainage basins (grey contours) are shown in the upper right corner. Drainage basins in white are not considered because they are associated to no or a very small ice shelf.

149 About 40% of the area covered by drainage basins feeding likely non-viable  
 150 shelves in 2300 is resting on bedrock that has been pressed below sea level due to the  
 151 weight of accumulating ice mass over thousands of years. Such low bedrock is one of  
 152 the necessary conditions for the marine ice sheet and ice cliff instabilities, which both

153 could trigger rapid mass loss episodes from the ice sheet to the ocean [7–10]. Likely  
154 non-viability of the associated ice shelves thus represents a theoretical potential for  
155  $\sim 10$  m of long-term sea-level rise, when aggregating the volume above flotation of  
156 these basins. This is an upper estimate as the occurrence of these instabilities also  
157 depends on other factors, notably the gradient of the bed slope [8] or the presence of  
158 high cliffs [41].

## 159 Drivers of non-viability

160 The link between the rate of ice shelves becoming non-viable and the rate of global  
161 warming could support the hypothesis that the viability of ice shelves is directly linked  
162 to an atmospheric temperature threshold [19, 20, 42]. However, global atmospheric  
163 warming is only one of multiple symptoms of climate change, other ones being for  
164 example ocean warming and changes in the ocean circulation. Using our holistic per-  
165 spective, we investigate more thoroughly the mechanisms triggering non-viability. This  
166 is done for every member of our ensemble, by quantifying the relative contribution of  
167 each mass flux to the ice-shelf mass loss at the date when non-viability is reached.

168 The ocean is by far the main driver for reaching non-viability (Fig. 3) and the  
169 surface mass balance has a much smaller influence. In both scenarios, basal melting  
170 explains more than half of the mass loss needed to reach non-viability for all ice shelves  
171 that reach non-viability. For the high-emission scenario, this is not surprising as a  
172 steep increase in basal melting starts around 2100 (Fig. S5). Nevertheless, we could  
173 not pinpoint a given ocean temperature threshold for non-viability.

174 The surface mass balance has a lower influence on non-viability. In the low-emission  
175 scenario, the surface mass balance does not lead to mass loss in any ice shelf at  
176 the moment of reaching non-viability and rather counteracts mass loss by 15% on  
177 average, confirming that an increase in accumulation prevails [13]. In the high-emission  
178 scenario, the surface mass balance leads to mass loss at the moment of reaching

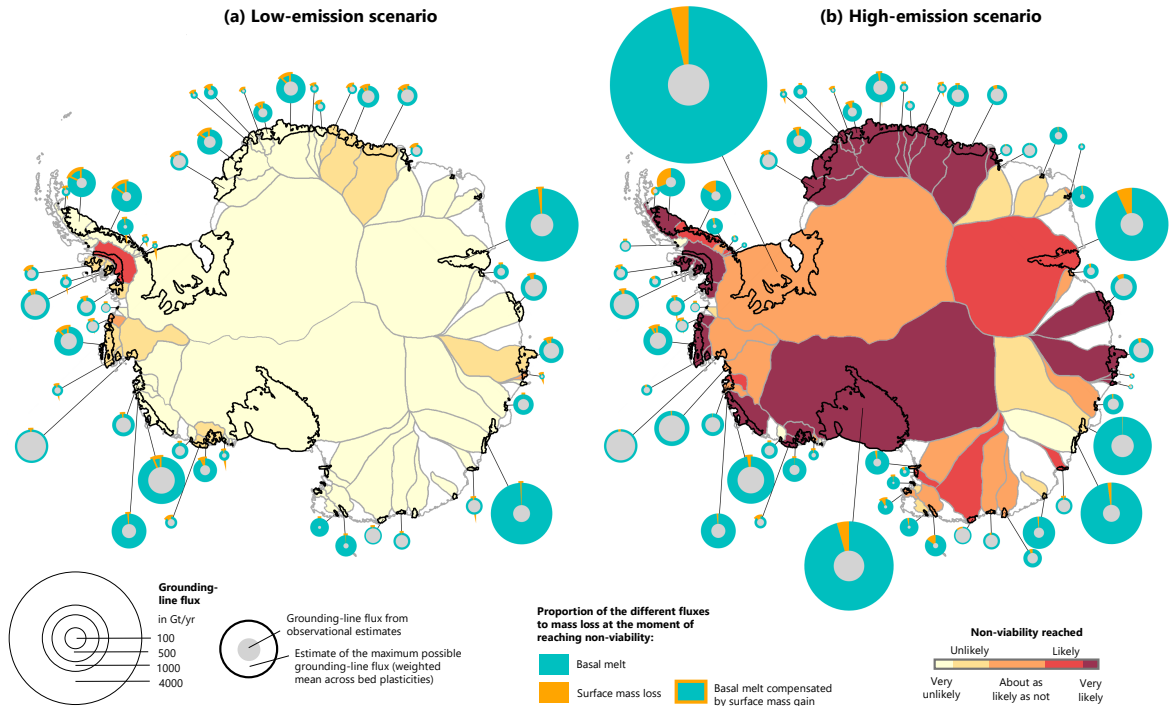


**Fig. 3 Relative importance of the different mass fluxes to reaching non-viability.** Average ratio between basal melt (blue) and surface mass balance (orange), respectively, and the maximal grounding-line flux at the moment when non-viability is reached for (a) the low-emission scenario and (b) the high-emission scenario. Circles are only shown if at least one ensemble member reaches non-viability before 2300. The grey circle represents the reference grounding-line flux and the area of the pie chart represents the upper-grounding line flux estimate (represented by a weighted mean of the estimates across bed plasticities). The ice shelves and associated drainage basins are colored based on the non-viability likelihood in 2300, as in Fig. 2.

179 non-viability for 60% of the ice shelves, but contributing on average only 2.5% to  
 180 non-viability for these ice shelves, with a maximum at 50% for the remains of Larsen B.

181 Zooming in on the main hot-spot regions of current high basal melt and prone to  
 182 marine ice-sheet instability (Pine Island and Thwaites ice shelves in the Amundsen  
 183 Sea and Totten and Moscow University ice shelves in East Antarctica), none of them  
 184 is likely non-viable by 2300. The probability is higher for Pine Island and Thwaites ice  
 185 shelves (about as likely as not), where the upper estimate for the grounding-line flux  
 186 is only slightly higher than the present flux, while Totten and Moscow University need  
 187 a large increase in mass loss to reach non-viability. On the one hand, this is somehow

188 consistent with the mechanism of marine ice-sheet instability: the weakening of an ice  
189 shelf increases the grounding-line flux, which decreases the mass of the grounded ice  
190 sheet but brings more mass to the ice shelf. This means, maybe counter-intuitively,  
191 that a marine ice-sheet instability would support the viability of an ice shelf, at least  
192 for some time, as long as there remains substantial amounts of grounded ice upstream.  
193 On the other hand, we emphasise that our approach results in a latest bound for  
194 non-viability and does not rule out an actual collapse occurring earlier, for example  
195 through hydrofracturing or damage and rifting, as suggested e.g. for Thwaites ice shelf  
196 [43, 44], or through long-term thinning.

## 197 **Implications**

198 Our results show that current choices to change emission pathways could significantly  
199 impact the likelihood of long-term loss of most Antarctic ice shelves. The viability of  
200 ice shelves strongly depends on the emission scenario, as only one ice shelf becomes  
201 likely or very likely non-viable by 2300 in the low-emission scenario versus 59% in the  
202 high-emission scenario. This difference between scenarios is particularly visible after  
203 2085, due to basal melting substantially increasing across all ice shelves around this  
204 date in the high-emission scenario (Fig. S5-S6). Nevertheless, this does not mean that  
205 the emission pathway leading to 2085 is not relevant to ice-shelf viability as increased  
206 basal melting is likely a lagged response to global atmospheric warming and therefore  
207 a consequence of emissions happening already earlier in the century (Fig. S1).

208 Although our non-viability estimate already presents a bleak outlook for the future  
209 of ice shelves, their actual collapse could occur even sooner. Our definition of non-  
210 viability represents the latest limit for viability as it is bound by an extreme mass gain  
211 from the ice sheet and minimal mass loss from calving. However, mass gain through  
212 the grounding-line flux will not necessarily reach its upper limit, which inherently  
213 integrates the effect of damage, rifting and hydrofracturing. Also, mass loss through

214 calving is projected to increase in the future for mid- and high-emission scenarios  
215 [39, 40]. Further, feedbacks between basal melting and ice geometry [45] or between  
216 calving and basal melting [46] could affect the stability of the ice shelf and potentially  
217 slightly alter the conditions to reach non-viability.

218 We emphasise that our non-viability estimate does not correspond to the most  
219 likely timing of collapse through thinning, increasing damage, hydrofracturing or  
220 stronger calving rate, but to an upper bound of the time when ice shelf shrinking  
221 becomes inevitable. Modelling tools are not ready yet for accurately simulating the  
222 prognostic interplay between these processes over multiple centuries, but we are con-  
223 fident that an upper bound can be estimated using our approach. Our non-viability  
224 estimate can nonetheless be used as a proxy for the prior ice-shelf mechanical weak-  
225 ening required for hydrofracturing [25–27]. This can be compared to the estimates of  
226 surface hydrological conditions also required for hydrofracturing: the production of  
227 liquid water beyond firn saturation, as estimated in Jourdain et al. [36]. Following  
228 their method, the surface hydrological conditions become prone to hydrofracturing  
229 before non-viability is reached for all ice shelves (Fig. S2), indicating that ice shelves  
230 that weaken beyond non viability will likely quickly be exposed to hydrofracturing,  
231 and hence to an actual collapse.

232 On another aspect, our study further underlines the importance of the ocean for  
233 the present and future evolution of the Antarctic ice sheet. However, global climate  
234 models currently struggle to simulate accurate Southern Ocean properties [47, 48].  
235 Reducing biases in the simulation of the Southern Ocean in global climate models, e.g.  
236 by improving the representation of processes on the continental shelf or by including  
237 ice-ocean interactions more systematically [49, 50], is therefore crucial. This should  
238 be a priority of the climate research community to better apprehend future sea-level  
239 evolution and the effect of meltwater on the oceanic circulation.

240 Finally, our results show that the risk of non-viability is a circum-Antarctic prob-  
241 lem, suggesting it to be a consequence of global temperature and circulation changes,  
242 rather than local changes. The likelihood of reaching non-viability is not tightly linked  
243 to one region as most ice shelves in the Bellingshausen, Amundsen and Ross seas, as  
244 well as in Dronning Maud Land, but also a few large ice shelves in East Antarctica are  
245 at risk of becoming non-viable. The impact of the potential long-term ice-shelf loss  
246 is strong in particular in the Bellingshausen, Amundsen and Ross seas. There, most  
247 of the associated drainage basins rest on bedrock below sea level and have a sea-level  
248 rise potential of several meters on the long term [51].

## 249 **Methods**

### 250 **Topography and boundaries of individual ice shelves**

251 The boundaries used to define the 64 largest ice shelves of Antarctica are the ones  
252 used in the Ice sheet Mass Balance Intercomparison Exercise (IMBIE) [52]. The ice  
253 topography is taken from BedMachine-Antarctica, version 2 [53]. All datasets are  
254 regrided to a 4-km stereographic grid to limit computational cost. This resolution is a  
255 reasonable compromise to represent the different components while keeping a balance  
256 between too high or too low confidence in the chosen resolution of the processes. For  
257 example, the grounding-line flux is inferred from the ice-sheet Elmer/Ice model at the  
258 kilometer-scale, the basal melt parameterisations were calibrated on ocean simulations  
259 at 5-8 km resolution, and the surface mass balance was downscaled from 35 km output.  
260 To minimise grounding-line imprecisions, we work with an “ice-shelf concentration”,  
261 which describes the fraction of a cell covered by ice-shelf parts. This allows us to  
262 better account for points near the grounding line than if we would only consider cells  
263 completely covered by ice shelves.

## 264 **Forcing**

265 The ocean and atmosphere forcing are based on the outputs from seven models from  
266 the sixth phase of the Coupled Model Intercomparison Project (CMIP6 [35]) covering  
267 1850 to 2300, under the Shared Socio-economic Pathways SSP1-2.6 (low-emission sce-  
268 nario) and SSP5-8.5 (high-emission scenario) that diverge from the historical period in  
269 2015: ACCESS-CM2, ACCESS-ESM1-5, CESM2-WACCM, CanESM5, IPSL-CM6A-  
270 LR, MRI-ESM2-0, UKESM1-0-LL. In the Supp. Info., we complement our main results  
271 with six additional models (CESM2, CNRM-CM6-1, CNRM-ESM2-1, GFDL-CM4,  
272 GFDL-ESM4, MPI-ESM1-2-HR) and the mid-emission scenario SSP2-4.5, which were  
273 only run until 2100. Conclusions until 2100 remain robust using the larger model  
274 ensemble (Fig. S7).

## 275 **Ice-shelf mass balance**

276 Our results are based on the analysis of the different contributors to the ice-shelf mass  
277 balance: the basal mass balance, the surface mass balance, the calving flux and the  
278 grounding-line flux (Fig. S3 to S6). If the ice-shelf mass balance becomes negative and  
279 remains negative until 2300, non-viability is reached.

## 280 **Basal mass balance**

281 Ocean-induced sub-shelf melt and refreezing are computed by applying basal melt  
282 parameterisations to geometrical properties of the sub-shelf cavities and to ocean tem-  
283 perature and salinity profiles inferred from yearly climate model output in front of the  
284 different ice shelves. To prepare these profiles, we first interpolate the coarse climate  
285 model output to a 8 km stereographic grid and extrapolate properties horizontally  
286 from contiguous ocean points to the points not covered by the CMIP6 model grid  
287 [54]. We then horizontally average the continental shelf (bathymetry shallower than

288 1500 m) ocean properties within 50 km of the ice-shelf front to obtain a single poten-  
289 tial temperature profile and a single practical salinity profile in front of each ice shelf,  
290 like in Burgard et al. [37].

291 Directly taking the ocean properties from the CMIP6 models leads to very large  
292 biases in estimated melt rates, sometimes of the order of several hundreds of  $\text{Gt yr}^{-1}$ ,  
293 which would strongly affect projected melt rates. Instead, we correct the CMIP6  
294 temperature and salinity profiles of individual ice shelves by subtracting the simulated  
295 1997–2014 average and adding a present-day estimate constrained by observations:  
296 either the climatology proposed for the Ice-Sheet Model Intercomparison Project for  
297 CMIP6 (ISMIP6) [55], or the output from a present-day ocean model hindcast forced  
298 by an atmospheric reanalysis [16]. We use these two different present-day estimates  
299 because some regions, such as Dronning Maud Land or the southwestern Weddell Sea,  
300 are not well covered by observations and the interpolated values given in the ISMIP6  
301 climatology are thus not necessarily reliable. For every ice shelf, we compute the  
302 difference between the observational sub-shelf melt estimates [11] and the melt inferred  
303 based on CMIP6 ocean properties corrected with the observational climatology on the  
304 one hand, and corrected with the model hindcast on the other hand. We select the  
305 correction where the median of this difference is lowest (see Sec. 6.1 in Supp. Info. for  
306 the resulting choices).

307 We use these corrected ocean profiles as input for six different basal melt  
308 parameterisations: (1) the linear-local parameterisation [56], (2) the quadratic-local  
309 parameterisation using a constant Antarctic slope [9, 37, 57], (3) the quadratic-local  
310 parameterisation using a local slope [37, 58, 59], (4) the plume parameterisation  
311 [60, 61], (5) the box parameterisation [62], and (6) the neural-network parame-  
312 terisation introduced in [38]. The physics-based parameterisations (1) to (5) are  
313 implemented as described in Burgard et al. [37], except a modified method to infer the  
314 depth of the plume origin. More details in Sec. 6.2 of the Supp. Info.

315 All of these parameterisations depend on one or two calibration parameters. Due  
316 to the low number of matching observational estimates of ocean properties and sub-  
317 shelf melt, we use cavity-resolving ocean simulations produced with the NEMO ocean  
318 model (Nucleus for European Modelling of the Ocean [63]) at  $0.25^\circ$  of resolution for  
319 the calibration (i.e. a resolution of 8 km in both directions at  $70^\circ$  S), as in previous  
320 studies [37, 38]. To reduce the calibration uncertainty, we calibrate the parameteri-  
321 sations using simulations covering both present-like and warmer ocean conditions. In  
322 addition to the ensemble of four present-day global simulations used for calibration in  
323 [37, 38], we use a global 70-year ocean simulation in conditions plausible by the late  
324 23<sup>rd</sup> century in the SSP5-8.5 scenario [16], and three circum-Antarctic simulations: a  
325 hindcast over 1982–2014 driven by a reanalysis and two projections over 2014–2100  
326 under the SSP5-8.5 scenario (see description in Sec. 6.3 in Supp. Info.). The two lat-  
327 ter projections differ by the choice of including the runoff from the ice-sheet surface  
328 in one and not in the other. For the physics-based parameterisations (1) to (5), we  
329 calibrate the parameter(s) to obtain the minimal root-mean-squared-error of the inte-  
330 grated ice-shelf melt across time and ice shelves (same method as Burgard et al. [37]).  
331 For the neural network, we calibrate the parameters to obtain the minimal root-mean-  
332 squared-error of the melt on the grid-cell level over time and space (same method as  
333 Burgard et al. [38]). The resulting parameters for the physics-based parameterisations  
334 are shown in Table S2 in the Supp. Info.

### 335 **Surface mass balance**

336 To estimate the atmospheric term contributing to the ice-shelf mass balance, we com-  
337 pute the Surface Mass Balance (SMB) as the difference between accumulation and  
338 ablation of mass at the surface. We do not directly use the SMB from the climate  
339 models because their overly low resolution is not sufficient to represent the topography  
340 of Antarctic ice shelves and because they usually do not represent the polar physical

341 processes needed to simulate the SMB evolution. Instead, we rely on regional projec-  
342 tions performed with the hydrostatic atmospheric model MAR (*Modèle Atmosphérique*  
343 *Régional* [64]) forced by several climate models and emission scenarios. We refer to  
344 Kittel et al. [13] for exhaustive details on the model configuration used. The MAR  
345 simulations are forced by the climate models IPSL-CM6A-LR (1980–2014 historical  
346 and 2015–2300 SSP5-8.5) and UKESM1-0-LL (1980–2014 historical and 2015–2100  
347 for both SSP1-2.6 and SSP5-8.5). More MAR simulations are available for three of  
348 the six additional CMIP6 models used until 2100 in the Supp. Info. For the other  
349 CMIP6 models, scenarios, or periods not covered by the MAR simulations, we use the  
350 SMB emulation trained with the aforementioned MAR simulations, as described and  
351 evaluated in Jourdain et al. [36]. These emulations are based on the changes in yearly  
352 surface air temperatures, as simulated in the corresponding CMIP6 simulations, and  
353 on physical and statistical relationships. A summary of the models, periods and sce-  
354 narios associated with simulated or emulated SMB is shown in Table S1 in the Supp.  
355 Info.

356 Rainfall, sublimation and deposition are taken into account in the SMB simu-  
357 lated by MAR as it accounts for the difference between accumulation (snowfall, liquid  
358 precipitation, and deposition) and ablation (runoff and sublimation). The emulation  
359 method, however, is applied to CMIP simulations not downscaled with MAR and  
360 assumes that rainfall plays a negligible role in generating runoff compared to surface  
361 melt [30, 36]. This assumption is supported by the extended MAR simulation under  
362 the highest emission scenario, which shows that rainfall remains a minor component  
363 of liquid production across all ice shelves until 2100, contributes less than 10% by  
364 2200, and becomes significant only locally by 2300—after most ice shelves have sur-  
365 passed their viability thresholds. As such, omitting rainfall leads to a conservative

366 estimate of ice shelf non-viability, consistent with our treatment of other fluxes. Sim-  
367 ilarly, sublimation and deposition are neglected in the emulation method, as they are  
368 not expected to substantially affect future mass balance [13].

369 Although the MAR resolution of 35 km represents a significant improvement com-  
370 pared to the resolution of climate models, this resolution is still not sufficient to  
371 represent the smallest ice shelves. Following previous statistical downscaling over  
372 Greenland [65] or Antarctica [66], we downscale the 35-km outputs to the common  
373 4-km grid. The method consists of a bi-linear interpolation to 4-km, followed by a cor-  
374 rection based on the local gradient of the interpolated variable with altitude, defined  
375 from the 4 closest neighbours.

### 376 **Calving flux**

377 There is no parameterisation estimating the evolution of the calving flux without the  
378 use of an ice-sheet model and our confidence in existing methods used to parameterise  
379 iceberg calving is limited. As a consequence, to include a lower boundary for calving,  
380 we set the calving flux to zero.

381 Instead of assuming the calving flux to be zero, it can also be assumed that ice-  
382 berg calving will remain constant or increase in the future, as suggested by previous  
383 studies for most scenarios [39, 40]. To investigate the influence of this assumption, we  
384 repeated the analysis assuming a constant calving flux for each ice shelf based on the  
385 observational steady-state estimates of Davison et al.[11] as a lower boundary instead  
386 of fixing it to zero. This leads to a slightly higher number of non-viable ice shelves  
387 by 2300, with 69% of the ice shelves at likely or very likely non-viable for the high-  
388 emission scenario (instead of 59%), and highlights the role of calving for the mass  
389 balance of a range of small ice shelves. It does, however, not substantially alter the  
390 main conclusions of our study. More details on this analysis and associated figures  
391 can be found in the Sec. 4 of the Supp. Info.

392 **Grounding-line flux**

393 The mass flux feeding the ice shelf from the grounded ice sheet (hereafter grounding-  
394 line flux) is mainly modulated by the buttressing arising from the contact of the ice  
395 shelves with ice rises, rumples, and lateral margins. To estimate an upper limit for the  
396 grounding-line flux, we therefore estimate the grounding-line flux occurring when no  
397 ice shelf is present downstream of the grounding line, the limit between grounded ice  
398 sheet and floating ice shelf. To do so, we conduct simulations similar to the Antarctic  
399 BUttrressing Model Intercomparison Project (ABUMIP) [67].

400 We conduct this experiment with the Finite Element ice-sheet and ice flow model  
401 Elmer/Ice [68], using the 2D Shallow-Shelf approximation to simulate the ice flow  
402 [e.g. 69–71]. We consider the present geometry from BedMachine-v2 [53] and invert  
403 for basal friction and ice viscosity parameters that allow for the ice flow model to best  
404 match observations of surface velocities [69–71]. This method enables, by construction,  
405 the simulated geometry and ice velocity to be as close as possible to present-day  
406 observations (see Sec. 6.4 in Supp. Info.).

407 From there, we recompute diagnostic ice flow responses with and without ice  
408 shelves as well as the corresponding grounding-line flux. We use the following  
409 Weertman friction law:

$$\tau_b = C_m |\mathbf{u}|^{1/m-1} \mathbf{u} \quad (1)$$

410 with  $C_m$  the friction parameter and  $m \in [1 - \infty]$  where increasing values of  $m$  are  
411 characteristic of a more plastic bed. We first conducted the inversion with  $m = 1$  but  
412 it has been proven that larger values might be more realistic in some regions like the  
413 Amundsen ( $m = 5$  in [72]). We therefore conduct diagnostic experiments with and  
414 without ice shelves accounting for  $m = [1, 3, 5]$  (and adjusting for  $C_m$ ) to assess the  
415 sensitivity to the friction law [73]. The impact of the value of  $m$  is relatively different  
416 basin to basin but our results align well with the sensitivity test of Gudmundsson et

417 al. [73] where they show a grounding line flux about 50-100% higher with  $m = 3$  than  
418 with  $m = 1$ . The different bed plasticities are applied on the whole Antarctic ice sheet,  
419 giving us three possible grounding-line fluxes for each ice shelf. The weighting process  
420 then determines which parameterisation-model-plasticity combinations influence our  
421 viability limit most (see Fig. S15).

422 Using the BedMachine geometry including the ice shelves results in a reference  
423 total grounding-line flux for Antarctica ranging from 1843 to 2124  $\text{Gt yr}^{-1}$ , depend-  
424 ing on the value of  $m$ . This value is very close to observations ( $2048 \pm 149 \text{ Gt yr}^{-1}$   
425 [74]). This reference flux is multiplied by  $\sim 3.5$  to  $\sim 7$  when removing the ice shelves.  
426 While the removal of some ice shelves leads to a large increase in grounding-line flux  
427 (e.g. Ross, Filchner-Ronne, Amery, Moscow University, Totten), other glaciers ini-  
428 tially exhibiting high fluxes do not largely increase them after losing their ice shelves  
429 (e.g. Thwaites, Pine Island). This behavior is usually in agreement with the mapping  
430 of buttressing potential [4].

### 431 **Defining non-viability**

432 Non-viability is reached when the ice-shelf mass balance becomes negative at one date  
433 and all following ones. In other words, the non-viability limit defined here represents  
434 ocean and atmosphere conditions for which it is virtually impossible that an ice shelf  
435 maintains its current shape on the long term despite the grounding-line flux being  
436 maximal and the calving flux being minimal. The non-viability of an ice shelf in  
437 these conditions can therefore be considered as a conservative estimate with regard  
438 to ice dynamics. Importantly, we do not attempt to estimate the date at which an ice  
439 shelf disintegrates or reaches zero thickness: on the one hand, a slight imbalance can  
440 make the ice shelf thin very slowly, and on the other hand, the actual ice flow from  
441 the grounded ice sheet would be smaller than in our estimate, making the mass loss

442 faster. Furthermore, as previously mentioned, hydrofracturing, damage and rifting  
443 may induce quick collapse of an ice shelf once it has lost enough mass.

444 We assess the viability of ice shelves with their current extent. If mass loss at the  
445 surface and at the base is large enough, an ice shelf will tend to get thinner. This  
446 may unpin the ice shelf, increase damage, and overall reduce buttressing, which can in  
447 turn increase the ice flow across the grounding line and potentially keep the ice shelf  
448 viable through compensation. As these dynamical effects remain difficult to represent  
449 in ice-sheet models, we place ourselves in the extreme case of a maximal ice-shelf mass  
450 gain through increased mass flux from the grounded ice sheet, and minimal mass loss  
451 through calving.

452 To confirm that our results remain valid for plausible grounding-line retreat beyond  
453 the current ice-sheet geometry, we repeated the analysis on two plausible future ice-  
454 sheet geometries, namely for 2100 and 2150, which lie in the period where most  
455 ice shelves become non-viable (see "Reaching non-viability") and have therefore the  
456 highest potential to influence our conclusions. These future ice-sheet geometries were  
457 simulated using the ice-sheet model Elmer/Ice forced by SSP5-8.5 output from IPSL-  
458 CM6A-LR. This is a model with comparably higher climate sensitivity [75] and  
459 integrates, among others, the effect on the grounding-line flux of (1) a possible increase  
460 in precipitation on the grounded ice sheet, (2) retreating grounding lines, and (3)  
461 ice-shelf thinning. The results of this new analysis are shown in Fig. S10. Overall,  
462 the conclusions are not significantly altered. In both geometries, the number of likely  
463 non-viable ice shelves by 2150 (26 in the 2100 geometry and 31 in the 2150 geom-  
464 etry) and by 2300 (43 in the 2100 geometry and 46 in the 2150 geometry) is equal  
465 or higher than the numbers inferred for the present geometry in the original analy-  
466 sis. This suggests that our initial estimates are indeed on the conservative side and  
467 remain valid even for plausible future ice-sheet geometries, probably because longer  
468 grounding lines, resulting from grounding-line retreat, and associated grounding-line

469 flux are compensated by increased mass loss at the base and the surface of the ice  
470 shelves due to their increased area. More details and associated figures can be found  
471 in Sec. 5 of the Supp. Info.

## 472 **Constraining the uncertainty**

473 The use of multiple combinations of CMIP6 models, basal melt parameterisations,  
474 and bed plasticities gives a large ensemble of possible ice-shelf mass balance evolu-  
475 tions for individual ice shelves. To constrain our analysis to a plausible ensemble for  
476 every ice shelf, we weight the different combinations based on the comparison of their  
477 historical period to the observational ice-shelf mass balance [11]. To also account for  
478 the likelihood of future warming in individual CMIP6 models, these weights are then  
479 multiplied by another weight accounting for the plausibility of the model equilibrium  
480 climate sensitivity [36, 76]. For information, the distribution of the weights per ice  
481 shelf and uncertainty dimension are shown in Fig. S13, S14 and S15 in the Supp. Info.

The weight describing the proximity of the historical simulation to observational estimates is inferred using Bayesian calibration similarly to Coulon et al. [40]. For a given ensemble member  $i$  (across the model-parameterisation-bed plasticity ensemble), the score  $s_i$  is computed as follows, for each ice-shelf separately:

$$s_i = \exp\left(-0.5 \frac{(MB_{\text{mod}, i} - MB_{\text{obs}})^2}{\sigma_{\text{mod}, i}^2 + \sigma_{\text{obs}}^2}\right) \quad (2)$$

482 where  $MB_{\text{mod}}$  and  $MB_{\text{obs}}$  are the simulated and observational ice-shelf mass bal-  
483 ance estimates respectively and  $\sigma_{\text{obs}}$  and  $\sigma_{\text{mod}}$  are the observational and structural  
484 errors. The observational ice-shelf mass balance is calculated from the 1997–2014  
485 mean estimates of Davison et al. [11] for basal mass balance, surface mass balance and  
486 grounding-line flux. We use their steady state calving flux rather than their 1997-2014  
487 mean calving flux because this is more consistent with a fixed calving front given that

488 we assess the viability of ice shelves in their current shape, while the actual 1997–2014  
489 calving flux is largely associated with changes in ice-shelf area. We use the 1997–  
490 2014 mean rather than interannual values because it is considered as a more robust  
491 observational estimate. The observational uncertainty  $\sigma_{\text{obs}}$  is the time-average of the  
492 square root of the sum of the squared uncertainties provided by Davison et al. [11] for  
493 individual mass fluxes. The structural error  $\sigma_{\text{mod}}$  is estimated by taking the standard  
494 deviation over time and averaging it across the model-parameterisation-bed plasticity  
495 space. From the score, we can then infer a normalised weight, by dividing each  $s_i$  by  
496 the sum of  $s_i$  across the ensemble. Finally, we set the weight to zero if the calving esti-  
497 mate surpasses the maximum estimate of the grounding-line flux as this would mean  
498 that the ice shelf is not viable even without basal melt, which is not realistic.

499 The weight describing the plausibility of the equilibrium climate sensitivity of  
500 each climate model is taken from Jourdain et al. [36]. These weights represent the  
501 probability, for a given climate model, of a skew-normal distribution fitted to obtain  
502 the 5<sup>th</sup>, 50<sup>th</sup> and 95<sup>th</sup> percentiles at an equilibrium climate sensitivity of 2.0, 3.0 and  
503 5.0°C, as expected from multiple lines of evidence [76].

504 All metrics presented in this study take the resulting weights into account. In par-  
505 ticular, we take these weights into account when estimating the likelihood of reaching  
506 non-viability, using the definitions commonly used in the IPCC reports [77]: very  
507 unlikely, unlikely, as likely as not, likely, and very likely (respectively 0-10%, 10-33%,  
508 33-66%, 66-90%, 90-100% weighted probability across the large ensemble of reaching  
509 non-viability).

510 **Supplementary information.** Supplementary Information is available for this  
511 paper. Correspondence and requests for materials should be addressed to  
512 clara.burgard@locean.ipsl.fr.

513 **Acknowledgements.** Most of the computations presented in this paper were  
514 performed using the GRICAD infrastructure (<https://gricad.univ-grenoble-alpes.fr>),

515 which is supported by Grenoble research communities. The NEMO simulations were  
516 performed using HPC resources from GENCI–TGCC (MISOCS project, allocation  
517 A0140106035). The ocean data processing and emulation of MAR simulations were  
518 performed on the IPSL Data and Computing Center (ESPRI).

## 519 **Declarations**

## 520 **Funding**

521 This research was funded by the DEEP-MELT project (IRGA Pack IA 2021-  
522 2022) supported by MIAI @ Grenoble Alpes (ANR-19-P3IA-0003), by the European  
523 Union’s Horizon 2020 research and innovation programme under grant agreements  
524 no. 869304 (PROTECT), 101003826 (CRiceS), 821001 (SO-CHIC), by the European  
525 Union’s Horizon Europe research and innovation programme under grant agreement  
526 no.101081193 (OptimESM) and 101060452 (OCEAN:ICE), as well as by Agence  
527 Nationale de la Recherche (ANR) - France 2030 as part of the PEPR TRACCS pro-  
528 gramme under grant number ANR-22-EXTR-0008 and ANR-22-EXTR-0010, and by  
529 ANR through the AIAI project (ANR-22-CE01-0014).

## 530 **Competing interests**

531 The authors declare no competing interests.

## 532 **Ethics approval and consent to participate**

533 Not applicable.

## 534 **Consent for publication**

535 Not applicable.

## 536 **Data and materials availability**

537 The data used to make the analysis and produce the figures can be found here: <https://doi.org/10.5281/zenodo.13768758>.  
538

## 539 **Code availability**

540 The code to extrapolate the CMIP6 data to the stereographic grid can be found here:  
541 <https://zenodo.org/records/12755910>. All other code used to produce the analysis  
542 and the figures is available on Github: [https://github.com/ClimateClara/scripts\\_for\\_](https://github.com/ClimateClara/scripts_for_review/)  
543 [review/](https://github.com/ClimateClara/scripts_for_review/).

## 544 **Author contribution**

545 CB and NCJ developed the original idea of this paper. CK carried out the MAR sim-  
546 ulations and part of the NEMO simulations used for the calibration of the basal melt  
547 parameterisations. NCJ carried out the MAR emulations and processed the CMIP6  
548 ocean outputs. PM carried out most of the NEMO simulations used for training. CM  
549 and JC carried out the present-day ice-sheet simulations and CM carried out the  
550 long-term future ice-sheet simulations and the ABUMIP-type experiments. CB cali-  
551 brated and applied the basal melt parameterisations. CB carried out all analyses and  
552 wrote the first draft of the manuscript. CB, NCJ, CK, CM, PM, JC all contributed  
553 to discussions on the design of the study, the analyses and the writing.

## 554 **References**

- 555 [1] Fox-Kemper, B. *et al.* *Ocean, Cryosphere and Sea Level Change. Climate Change*  
556 *2021: The Physical Science Basis. Contribution of Working Group I to the Sixth*  
557 *Assessment Report of the Intergovernmental Panel on Climate Change* (Cam-  
558 bridge University Press, Cambridge, United Kingdom and New York, NY, USA,  
559 2021).

- 560 [2] Doake, C. S. M., Corr, H. F. J., Rott, H., Skvarca, P. & Young, N. W. Breakup  
561 and conditions for stability of the northern Larsen Ice Shelf, Antarctica. *Nature*  
562 **391**, 778–780 (1998).
- 563 [3] Reese, R., Gudmundsson, G. H., Levermann, A. & Winkelmann, R. The far reach  
564 of ice-shelf thinning in Antarctica. *Nat. Clim. Change* **8**, 53–57 (2018).
- 565 [4] Fürst, J. *et al.* The safety band of antarctic ice shelves. *Nat. Clim. Change* **6**,  
566 479–482 (2016).
- 567 [5] Rignot, E. *et al.* Accelerated ice discharge from the Antarctic Peninsula following  
568 the collapse of Larsen B ice shelf. *Geophys. Res. Lett.* **31**, L18401 (2004).
- 569 [6] Scambos, T. A., Bohlander, J. A., Shuman, C. A. & Skvarca, P. Glacier accelera-  
570 tion and thinning after ice shelf collapse in the Larsen B embayment, Antarctica.  
571 *Geophys. Res. Lett.* **31** (2004).
- 572 [7] Weertman, J. Stability of the Junction of an Ice Sheet and an Ice Shelf. *J.*  
573 *Glaciol.* **13**, 3–11 (1974).
- 574 [8] Schoof, C. Ice sheet grounding line dynamics: Steady states, stability, and  
575 hysteresis. *J. Geophys. Res.* **112**, F03S28 (2007).
- 576 [9] DeConto, R. & Pollard, D. Contribution of Antarctica to past and future sea-level  
577 rise. *Nature* **531**, 591–597 (2016).
- 578 [10] Bassis, J. N. *et al.* Stability of ice shelves and ice cliffs in a changing climate.  
579 *Annu. Rev. Earth Planet. Sci.* **52** (2024).
- 580 [11] Davison, B. *et al.* Annual mass budget of Antarctic ice shelves from 1997 to 2021.  
581 *Sci. Adv.* **9**, eadi0186 (2023).

- 582 [12] Paolo, F., Fricker, H. & Padman, L. Volume loss from Antarctic ice shelves is  
583 accelerating. *Science* **348**, 327–331 (2015).
- 584 [13] Kittel, C. *et al.* Diverging future surface mass balance between the Antarctic ice  
585 shelves and grounded ice sheet. *Cryosphere* **15**, 1215–1236 (2021).
- 586 [14] van Wessem, J. M., van den Broeke, M. R., Wouters, B. & Lhermitte, S. Variable  
587 temperature thresholds of melt pond formation on antarctic ice shelves. *Nat.*  
588 *Clim. Change* **13**, 161–166 (2023).
- 589 [15] Timmermann, R. & Hellmer, H. H. Southern Ocean warming and increased  
590 ice shelf basal melting in the twenty-first and twenty-second centuries based on  
591 coupled ice-ocean finite-element modelling. *Ocean Dyn.* **63**, 1011–1026 (2013).
- 592 [16] Mathiot, P. & Jourdain, N. Southern Ocean warming and Antarctic ice shelf  
593 melting in conditions plausible by late 23rd century in a high-end scenario. *Ocean*  
594 *Sci.* **19**, 1595–1615 (2023).
- 595 [17] Robin, G. d. Q. & Adie, R. J. *The Ice Cover*, 100–117 (Butterworths, London,  
596 1964).
- 597 [18] Mercer, J. H. West Antarctic ice sheet and CO<sub>2</sub> greenhouse effect: a threat of  
598 disaster. *Nature* **271**, 321–325 (1978).
- 599 [19] Vaughan, D. & Doake, C. Recent atmospheric warming and retreat of ice shelves  
600 on the Antarctic Peninsula. *Nature* **379**, 328–331 (1996).
- 601 [20] Cook, A. & Vaughan, D. Overview of areal changes of the ice shelves on the  
602 Antarctic Peninsula over the past 50 years. *Cryosphere* **4**, 77–98 (2010).
- 603 [21] Scambos, T. A., Hulbe, C., Fahnestock, M. & Bohlander, J. The link between cli-  
604 mate warming and break-up of ice shelves in the Antarctic Peninsula. *J. Glaciol.*

- 605       **46**, 516–530 (2000).
- 606 [22] Scambos, T., Hulbe, C. & Fahnestock, M. *Climate-Induced Ice Shelf Disinte-*  
607 *gration in the Antarctic Peninsula*, 79–92 (American Geophysical Union (AGU),  
608 2003).
- 609 [23] Skvarca, P., De Angelis, H. & Zakrajsek, A. F. Climatic conditions, mass balance  
610 and dynamics of Larsen B ice shelf, Antarctic Peninsula, prior to collapse. *Ann.*  
611 *Glaciol.* **39**, 557–562 (2004).
- 612 [24] Lai, C.-Y. *et al.* Vulnerability of Antarctica’s ice shelves to meltwater-driven  
613 fracture. *Nature* **584**, 574–578 (2020).
- 614 [25] Shepherd, A., Wingham, D., Payne, T. & Skvarca, P. Larsen ice shelf has  
615 progressively thinned. *Science* **302**, 856–859 (2003).
- 616 [26] Lhermitte, S., Wouters, B. & HiRISE Team. *The triggers for Conger Ice Shelf*  
617 *demise: Long-term weakening vs. short-term collapse*, EGU–16400 (2023).
- 618 [27] Walker, C. *et al.* The Multi-decadal Collapse of East Antarctica’s Conger-Glenzer  
619 Ice Shelf. *Nature Geoscience* **17**, 1240–1248 (2024).
- 620 [28] Wild, C. T. *et al.* Weakening of the pinning point buttressing Thwaites Glacier,  
621 West Antarctica. *Cryosphere* **16**, 397–417 (2022).
- 622 [29] Lenaerts, J. T. M. *et al.* Climate and surface mass balance of coastal West  
623 Antarctica resolved by regional climate modelling. *Ann. Glaciol.* **59**, 29–41  
624 (2018).
- 625 [30] Donat-Magnin, M. *et al.* Future surface mass balance and surface melt in the  
626 Amundsen sector of the West Antarctic Ice Sheet. *Cryosphere* **15**, 571–593 (2021).

- 627 [31] Rignot, E., Vaughan, D. G., Schmeltz, M., Dupont, T. & MacAyeal, D. Accel-  
628 eration of Pine island and Thwaites glaciers, west Antarctica. *Ann. Glaciol.* **34**,  
629 189–194 (2002).
- 630 [32] Rignot, E., Mouginot, J., Morlighem, M., Seroussi, H. & Scheuchl, B.  
631 Widespread, rapid grounding line retreat of Pine Island, Thwaites, Smith, and  
632 Kohler glaciers, West Antarctica, from 1992 to 2011. *Geophys. Res. Lett.* **41**,  
633 3502–3509 (2014).
- 634 [33] Lhermitte, S. *et al.* Damage accelerates ice shelf instability and mass loss in  
635 Amundsen Sea Embayment. *Proc. Natl. Acad. Sci. U.S.A.* **117**, 24735–24741  
636 (2020).
- 637 [34] Seroussi, H. *et al.* Insights into the vulnerability of Antarctic glaciers from the  
638 ISMIP6 ice sheet model ensemble and associated uncertainty. *Cryosphere* **17**,  
639 5197–5217 (2023).
- 640 [35] Eyring, V. *et al.* Overview of the Coupled Model Intercomparison Project Phase 6  
641 (CMIP6) experimental design and organization. *Geosci. Model Dev.* **9**, 1937–1958  
642 (2016).
- 643 [36] Jourdain, N., Amory, C., Kittel, C. & Durand, G. Changes in Antarctic surface  
644 conditions and potential for ice shelf hydrofracturing from 1850 to 2200. *The*  
645 *Cryosphere* 1641—1674 (2025).
- 646 [37] Burgard, C., Jourdain, N., Reese, R., Jenkins, A. & Mathiot, P. An assessment of  
647 basal melt parameterisations for Antarctic ice shelves. *Cryosphere* **16**, 4931–4975  
648 (2022).
- 649 [38] Burgard, C. *et al.* Emulating Present and Future Simulations of Melt Rates at  
650 the Base of Antarctic Ice Shelves With Neural Networks. *J. Adv. Model. Earth*

- 651 *Syst.* **15**, e2023MS003829 (2023).
- 652 [39] Park, J.-Y. *et al.* Future sea-level projections with a coupled atmosphere-ocean-  
653 ice-sheet model. *Nat. Commun.* **14**, 636 (2023).
- 654 [40] Coulon, V. *et al.* Disentangling the drivers of future Antarctic ice loss with a  
655 historically calibrated ice-sheet model. *Cryosphere* **18**, 653–681 (2024).
- 656 [41] Morlighem, M. *et al.* The West Antarctic Ice Sheet may not be vulnerable to  
657 marine ice cliff instability during the 21st century. *Science Advances* **10**, eado7794  
658 (2024).
- 659 [42] Morris, E. M. & Vaughan, D. G. *Spatial and Temporal Variation of Surface*  
660 *Temperature on the Antarctic Peninsula And The Limit of Viability of Ice Shelves*,  
661 61–68 (American Geophysical Union (AGU), 2003).
- 662 [43] Benn, D. *et al.* Rapid fragmentation of Thwaites Eastern Ice Shelf. *The*  
663 *Cryosphere* **16**, 2545–2564 (2022).
- 664 [44] Wild, C. *et al.* Rift propagation signals the last act of the Thwaites Eastern Ice  
665 Shelf despite low basal melt rates. *Journal of Glaciology* **70**, e21 (2024).
- 666 [45] De Rydt, J. & Naughten, K. Geometric amplification and suppression of ice-shelf  
667 basal melt in West Antarctica. *Cryosphere* **18**, 1863–1888 (2024).
- 668 [46] Bradley, A. T., Bett, D. T., Dutrieux, P., De Rydt, J. & Holland, P. R. The  
669 Influence of Pine Island Ice Shelf Calving on Basal Melting. *J. Geophys. Res.*  
670 **127**, e2022JC018621 (2022).
- 671 [47] Beadling, R. *et al.* Representation of Southern Ocean Properties across Coupled  
672 Model Intercomparison Project Generations: CMIP3 to CMIP6. *J. Clim.* **33**,  
673 6555–6581 (2020).

- 674 [48] Heuzé, C. Antarctic Bottom Water and North Atlantic Deep Water in CMIP6  
675 models. *Ocean Sci.* **17**, 59–90 (2021).
- 676 [49] Smith, R. *et al.* Coupling the U.K. Earth System Model to Dynamic Mod-  
677 els of the Greenland and Antarctic Ice Sheets. *J. Adv. Model. Earth Syst.* **13**,  
678 e2021MS002520 (2021).
- 679 [50] Schmidt, G. *et al.* Anomalous Meltwater From Ice Sheets and Ice Shelves Is a  
680 Historical Forcing. *Geophys. Res. Lett.* **50**, e2023GL106530 (2023).
- 681 [51] Martin, D. F., Cornford, S. L. & Payne, A. J. Millennial-Scale Vulnerability of  
682 the Antarctic Ice Sheet to Regional Ice Shelf Collapse. *Geophys. Res. Lett.* **46**,  
683 1467–1475 (2019).
- 684 [52] Rignot, E. *et al.* Four decades of Antarctic Ice Sheet mass balance from  
685 1979–2017. *Proc. Natl. Acad. Sci. U.S.A.* **116**, 1095–1103 (2019).
- 686 [53] Morlighem, M. MEaSUREs BedMachine Antarctica, Version 2. (2020). Boulder,  
687 Colorado USA. NASA National Snow and Ice Data Center Distributed Active  
688 Archive Center.
- 689 [54] Jourdain, N. C. nicojourdain/CMIP6\_data\_to\_ISMIP6\_grid: v1.0 (v1.0). Tech.  
690 Rep., Zenodo (2024). URL <https://doi.org/10.5281/zenodo.12755910>.
- 691 [55] Jourdain, N. *et al.* A protocol for calculating basal melt rates in the ISMIP6  
692 Antarctic ice sheet projections. *Cryosphere* **14**, 3111–3134 (2020).
- 693 [56] Beckmann, A. & Goosse, H. A parameterization of ice shelf–ocean interaction  
694 for climate models. *Ocean Model.* **5**, 157–170 (2003).
- 695 [57] Holland, P., Jenkins, A. & Holland, D. The Response of Ice Shelf Basal Melting  
696 to Variations in Ocean Temperature. *J. Clim.* **21**, 2558–2572 (2008).

- 697 [58] Little, C. M., Gnanadesikan, A. & Oppenheimer, M. How ice shelf morphology  
698 controls basal melting. *J. Geophys. Res.* **114** (2009).
- 699 [59] Jenkins, A. *et al.* West Antarctic Ice Sheet retreat in the Amundsen Sea driven  
700 by decadal oceanic variability. *Nat. Geosci.* **11**, 733–738 (2018).
- 701 [60] Lazeroms, W., Jenkins, A., Gudmunsson, G. & van de Wal, R. Modelling present-  
702 day basal melt rates for Antarctic ice shelves using a parametrization of buoyant  
703 meltwater plumes. *Cryosphere* **12**, 49–70 (2018).
- 704 [61] Lazeroms, W., Jenkins, A., Rienstra, S. & van de Wal, R. An Analytical Deriva-  
705 tion of Ice-Shelf Basal Melt Based on the Dynamics of Meltwater Plumes. *J.*  
706 *Phys. Oceanogr.* **49**, 917–939 (2019).
- 707 [62] Reese, R., Albrecht, T., Mengel, M., Asay-Davis, X. & Winkelmann, R. Antarctic  
708 sub-shelf melt rates via PICO. *Cryosphere* **12**, 1969–1985 (2018).
- 709 [63] NEMO Team. NEMO ocean engine. *Scientific Notes of Climate Modelling Center*  
710 **27** (2019).
- 711 [64] Gallée, H. & Schayes, G. Development of a three-dimensional meso- $\gamma$  primi-  
712 tive equation model: katabatic winds simulation in the area of Terra Nova Bay,  
713 Antarctica. *Mon. Weather Rev.* **122**, 671–685 (1994).
- 714 [65] Franco, B., Fettweis, X., Lang, C. & Erpicum, M. Impact of spatial resolution on  
715 the modelling of the Greenland ice sheet surface mass balance between 1990–2010,  
716 using the regional climate model MAR. *Cryosphere* **6**, 695–711 (2012).
- 717 [66] Noël, B. *et al.* Higher Antarctic ice sheet accumulation and surface melt rates  
718 revealed at 2 km resolution. *Nat. Commun.* **14**, 7949 (2023).

- 719 [67] Sun, S. *et al.* Antarctic ice sheet response to sudden and sustained ice-shelf  
720 collapse (ABUMIP). *J. Glaciol.* **66**, 891–904 (2020).
- 721 [68] Gagliardini, O. *et al.* Capabilities and performance of Elmer/Ice, a new-  
722 generation ice sheet model. *Geosci. Model Dev.* **6**, 1299–1318 (2013).
- 723 [69] Brondex, J., Gillet-Chaulet, F. & Gagliardini, O. Sensitivity of centennial mass  
724 loss projections of the Amundsen basin to the friction law. *Cryosphere* **13**, 177–  
725 195 (2019).
- 726 [70] Klein, E. *et al.* Annual cycle in flow of Ross Ice Shelf, Antarctica: contribution  
727 of variable basal melting. *J. Glaciol.* **66**, 861–875 (2020).
- 728 [71] Mosbeux, C., Padman, L., Klein, E., Bromirski, P. & Fricker, H. Seasonal vari-  
729 ability in Antarctic ice shelf velocities forced by sea surface height variations.  
730 *Cryosphere* **17**, 2585–2606 (2023).
- 731 [72] Gillet-Chaulet, F. *et al.* Assimilation of surface velocities acquired between 1996  
732 and 2010 to constrain the form of the basal friction law under Pine Island Glacier.  
733 *Geophys. Res. Lett.* **43**, 10,311–10,321 (2016).
- 734 [73] Gudmundsson, G. H., Paolo, F. S., Adusumilli, S. & Fricker, H. Instantaneous  
735 Antarctic ice sheet mass loss driven by thinning ice shelves. *Geophys. Res. Lett.*  
736 **46**, 13903–13909 (2019).
- 737 [74] Rignot, E., Jacobs, S., Mouginot, J. & Scheuchl, B. Ice-shelf melting around  
738 Antarctica. *Science* **341**, 266–270 (2013).
- 739 [75] Meehl, G. *et al.* Context for interpreting equilibrium climate sensitivity and tran-  
740 sient climate response from the CMIP6 Earth system models. *Science Advances*  
741 **6**, eaba1981 (2020).

- 742 [76] Forster, P. *et al.* in *The Earth's energy budget, climate feedbacks, and climate*  
743 *sensitivity. Climate Change 2021: The Physical Science Basis. Contribution of*  
744 *Working Group I to the Sixth Assessment Report of the Intergovernmental Panel*  
745 *on Climate Change* (eds Masson-Delmotte, V. *et al.*) 923–1054 (Cambridge,  
746 United Kingdom and New York, NY, USA, 2021).
- 747 [77] Mastrandrea, M. *et al.* Guidance Note for Lead Authors of the IPCC Fifth  
748 Assessment Report on Consistent Treatment of Uncertainties. *Intergovernmental*  
749 *Panel on Climate Change (IPCC)* (2010). URL <http://www.ipcc.ch>.